Proceedings of the 11th World Congress in Mechanism and Machine Science
August 18~21, 2003, Tianjin, China
China Machinery Press, edited by Tian Huang

# Evaluation of a 4-Degree of Freedom Parallel Manipulator Stiffness

Charles CORRADINI, Jean-Christophe FAUROUX
LaRAMA, IFMA, Campus universitaire de Clermont-Ferrand / Les Cézeaux,
BP 265, 63175 AUBIERE Cedex, FRANCE
Tel: +33.(0)4.73.28.80.50 Fax: +33.(0)4.73.28.81.00 E-Mail: fauroux@ifma.fr

Sébastien KRUT, Olivier COMPANY
LIRMM, 161 rue Ada, 34392 Montpellier Cedex 5, FRANCE
Tel: +33.(0)4.67.41.85.74 Fax: +33.(0)4.67.41.85.00 E-Mail: company@lirmm.fr

**Abstract:** The H4 parallel robot is a new type of parallel machine with four degrees of freedom. The purpose of this work is to evaluate the H4 stiffness, that is to say the displacement response of the terminal travelling plate when it is submitted to a given force. Robot kinematics is described and information about parallel kinematics machine is given. Firstly, the experimental setup used to measure prototype stiffness is presented, which allows us to obtain real data and also to take into account geometry defaults and clearance between parts (backlash). Secondly, a Finite Element Analysis is described, including a multi-beam articulated model where all the joints are translated into displacement relaxations. Finally, results of both methods are compared and conclusions on the current robot design are drawn.

**Keywords:** Parallel Kinematics Machines, Stiffness, Compliance, FEA, H4 Robot

## 1 Introduction

The H4 parallel robot is a new type of parallel machine with four degrees of freedom. The possible motions of H4 prototype are three translations and one rotation about a given axis (Schroenflies motions subgroup), which is quite interesting for fast *pick-and-place* tasks as prototype Tool Controlled Point (TCP) acceleration can reach up to 10g.

Stiffness is a crucially important performance specification of Parallel Kinematics Machines (PKM). In order to get a real industrial machine, the H4 prototype must be optimised. Considering the long arms and bars it is made of, designers must be particularly careful with the machine stiffness, which has direct consequences on manipulation accuracy [1]. Several studies were performed by inventors to determine the geometrical model, the usable workspace and the forces in the machine components [2]. The work is divided into four parts:

- Firstly, robot geometry is defined and its kinematics is presented
- Secondly, experiments are performed on the H4 prototype and give real results, including geometry defaults and clearance between parts (backlash)
- Thirdly, a Finite Element Analysis is performed, with a multi-beam articulated model where all the joints are translated into displacement relaxations
- Finally, results of both methods are compared and conclusions on the current robot design are drawn.

Obtained numerical results are displacements for a given force. From these results, it is easier to derive what we call compliance defined by a displacement divided by a force. Compliance is inverse stiffness.

## 2 Robot Kinematics Description

Robot kinematics can be described by its joint and loop graph (figure 1) where each box stands for a revolute (R) or spherical (S) joint. Grey boxes represent actuated joints. Robot is made of four legs (actuator + forearm + two bars) of R-(S-S)$_2$ type. These legs link the robot frame to the 'H' shaped articulated travelling plate.

Robot practical design is extremely simple thanks to the use of direct drive motors. Bars are made from carbon fibre; arms, forearms and travelling plate are made from aluminium alloy. Before going further, robot geometry must be modelled. As depicted on figure 2: $P_i$ is a point belonging to $i^{th}$ actuator revolute axis ($i = 1..4$), $\boldsymbol{u_i}$ is the unitary vector defining the rotation axis, $A_{ij}$ is the centre of ball joint number $j$ on the actuator side ($j = 1..2$), $A_i$ is the middle of $A_{i1}$ and $A_{i2}$, $B_{ij}$ is the centre of ball joint number $j$ on the travelling plate side, $B_i$ is the middle of $B_{i1}$ and $B_{i2}$, $\boldsymbol{v_k}$ is unitary vector of revolute joint on side number $k$ of the travelling plate ($k = 1..2$ see figure 3), $C_k$ is the centre of the revolute joint on the side number $k$ of the travelling plate, $D$ is the TCP.

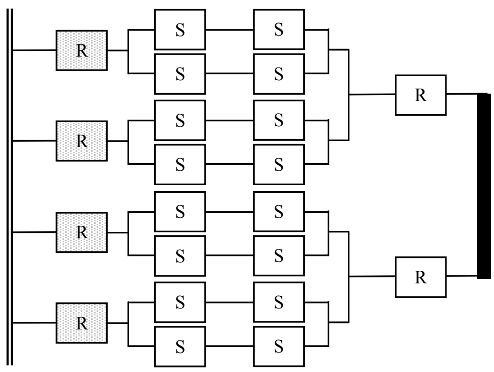


**Figure 1. H4 robot joint and loop graph**

H4 robot prototype was built according to the following simplifying hypotheses: all forearms have the same length $r$ and all bars have the same length $l$.

Geometrical constraints (these constraints are required to have TCP desired displacements *i.e.* three translations and one rotation about $z$ axis [3]): vector defined by $A_{i1}$ and $A_{i2}$ is collinear to $\boldsymbol{u}_i$, vector defined by $B_{i1}$ and $B_{i2}$ must be collinear to $\boldsymbol{u}_i$, $\boldsymbol{v}_1$ and $\boldsymbol{v}_2$ are collinear to $z$ axis.

As this robot is quite new, some explanations about its behaviour are now given. The robot is made of four "legs" linking the fixed part (with the reference frame visible in figure 2) to the travelling plate. The overall technology and working principle are identical to robot Delta [4]. The major improvement lays in the use of an articulated travelling plate instead of a rigid one. Its shape looks like the "H" letter. It is made of two lateral beams linked to the central bar by two revolute joints. Each leg is made of a forearm and a "spatial parallelogram" *i.e.* a four (theoretically planar) bar linkage with spherical joints, each side having the same length as the opposite one.

When the robot is assembled, lateral beams are parallel to each other. In such a configuration, spatial parallelograms are planar only if geometrical design rules are respected during the design stage. When the robot moves, except for singular configurations, the lateral beams remain parallel and spatial parallelograms planar. The end effector is linked to the central bar. Its possible displacements are three translations and one rotation about a given axis ($z$ for this prototype). This rotation is obtained by relative displacement of parts inside the articulated travelling plate (a video of running robot can be seen on LIRMM website[5]).

When robot components do not have their theoretical geometry due to bad manufacturing process or deformations linked to external forces applied to the robot, the travelling plate does not remain parallel when moving and lateral beams do not remain parallel to each other

To extend the end effector angular range (initially limited to ± 45 degrees) and to reach a 180-degree rotation capability in both directions, travelling plate design has been improved by adding a geared mechanical amplification system with a ratio of 4:1 that can be seen on figure 3. This device was removed during the experimental phase and not taken into account in FEM analysis and rough modeling.

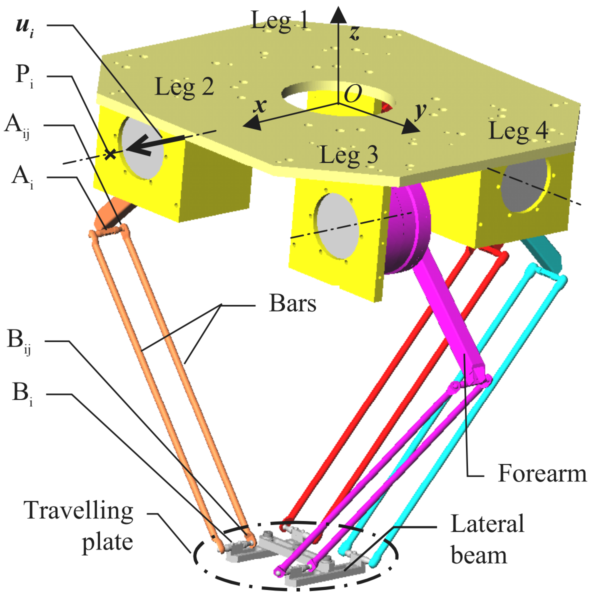


**Figure 2. Robot CAD model**

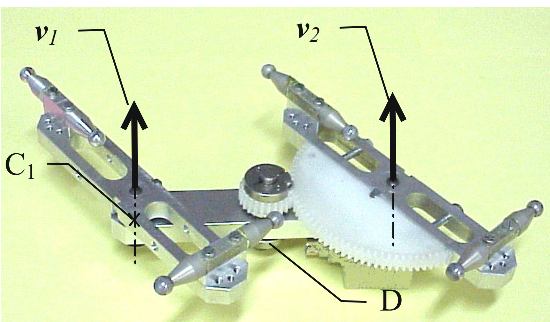


**Figure 3. Prototype travelling plate**

## 3 Stiffness Measuring

Stiffness measuring method requires common metrology devices. An external force is applied to TCP respectively along the axes of the reference frame $x$, $y$ and $z$. This force is measured by a load cell (see figure 4 for a scheme of a measurement when a force is applied along $z$). Applied loads were chosen ranging from 10 to 50 Newtons - reasonable loads with regards to the H4 current structure and possible applications (pick and place of small components). The resulting displacement of TCP is then measured in the direction of the three axes of the reference frame by three dial indicators. The practical setup can be seen on figure 5. During the experiments, actuators were powered and position controlled.

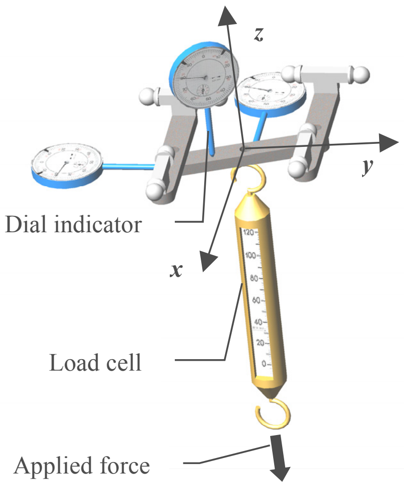


**Figure 4. Experimental setting scheme**

**Figure 5. Stiffness measuring operation**

Of course, the results of these measurements are valid only for the chosen pose. In our experimental case the chosen pose is when all actuators angle are equal to 45°. For these angles the central bar of the travelling plate is perpendicular to lateral beams.

TCP has four degrees of freedom, but stiffness must be given in six axes (3 translational and 3 angular). For this first work on this prototype, only translational stiffness is studied. Numerical results of this experiment are presented in section 5.

## 4 FEM Analysis

### 4.1 Finding material properties

The shape of nearly each part of the H4 prototype can be easily extracted from the existing CAD model of the robot, in particular beam cross sections. Concerning material, most of the parts are made of the classical 2024 aluminium alloy series (also known as AU4G).

The problem for bars is different. These parts were manufactured ten years ago by third party. It is impossible to have reliable information about their internal shape and material. From visual inspection, they seem to be made of carbon-epoxy composite material.

In order to get a precise material stiffness, a bar was tested on a tensile testing machine (figure 6). Due to the specific shape of the spherical joint external cage at each tip of the bar, dedicated fixtures in two halves had also to be milled.

The resulting traction curve was perfectly linear, as expected, and gave us traction strength against displacement. In order to find elasticity modulus, cross section is also needed. Unfortunately it is unknown because the sample bar must not be destroyed. The bar is assumed to be a hollow cylinder with a 2-millimetre thickness. Corresponding material properties can be found in Table 1.

### 4.2 FEM model

Our purpose is to create a simplified FEM model of the H4 robot in order to confirm stiffness behaviour. Consequently, we decided to start with a simple beam model. By doing so, complex shapes are neglected such

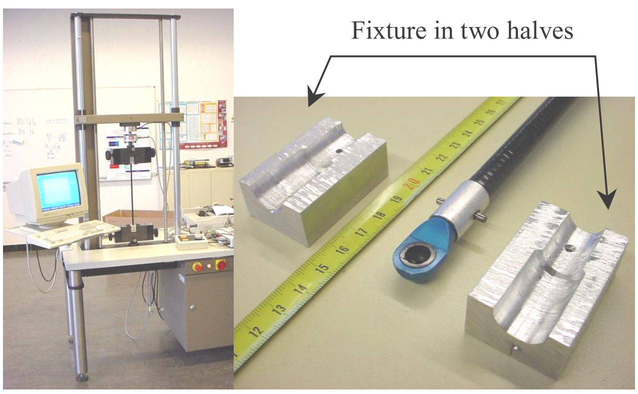


**Figure 6. Testing the bars**

| Part | Material | Elasticity modulus | Cross section (dimensions in millimetres) |
|---|---|---|---|
| Arm | Aluminium 2024 series | 74000 MPa | Square tube with round corners (Side 25, Thickness 2.5, Ext. radius 3, Int. radius 1) |
| Bar | Carbon Epoxy | 57700 MPa | Round tube ( External diameter 10.4, Thickness 2 ) |

**Table 1. Material properties for two robot parts**

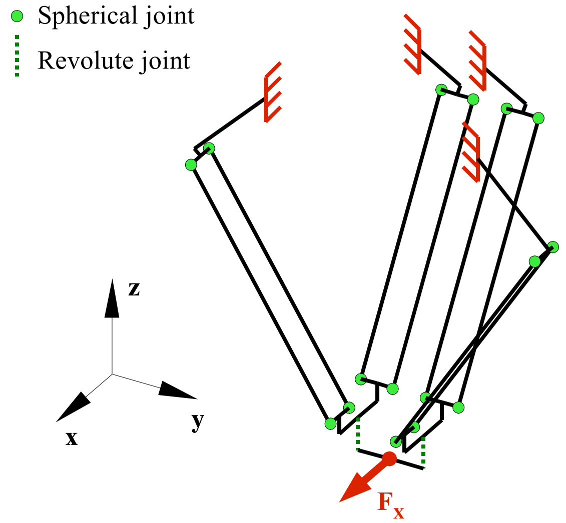


**Figure 7. Multi-beam articulated FEM model**

as conical fixtures of spherical joint or holes in end effector plates. This model will be refined in further work with a 3D model such as the one presented in [6].

An interesting point to notice is that FEM is an exact method for beams with constant cross section, which is our case [7]. This means we may represent a beam with only one element and still find exactly the same result as with material strength theory. Using this property, a model is constructed with 41 nodes and 44 beams of various cross sections (figure 7). In the real model, the top part of the arms is bolted to the rotor of the motors. As motors are considered to be fixed, the top part of the arms was not represented. One can notice that several beams are really short and thus do not meet the long beam hypothesis, but this should induce minor error in results. For creating the model, a FEM software dedicated to 3D beam structures [8] was used. Each node has 6 degrees of freedom: 3 translations $D_x$, $D_y$, $D_z$ and 3 rotation angles $R_x$, $R_y$, $R_z$ in local frame (figure 8). Three forces N, $T_y$, $T_z$ and three torques $M_x$, $M_y$, $M_z$ are applied to one node.

All the connected beams are welded by default, *i.e.* all the degrees of freedom on the common node are the same. For modelling joints, displacement relaxation is introduced, *i.e.* some displacements are not the same for both beams on the common node. Here are the two types of joints to model:

- spherical joint: translations are the same on each beam but not rotations
- revolute joint: all movements are the same but not rotation around the joint axis.

One should be careful with the bars that have a spherical joint on each tip. The software must be able to transform the beam element into a bar element with no self rotation around its longitudinal axis or else, reversing the

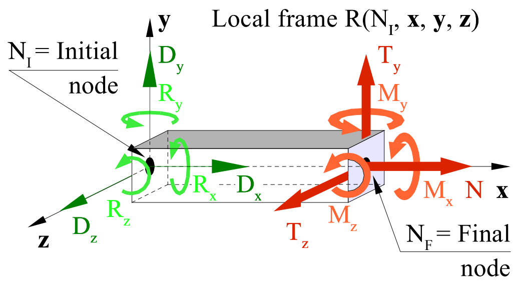


**Figure 8. A beam with nodal displacements and loads**

matrix of the FEM system leads to a null numerical pivot. From a practical point of view, this FEM model is very fast to solve (less than two seconds on a PIII 650 Mhz).

## 5 Results

All experimental and FEM results are summarised in figure 9 in three graphs, one for each force direction. Each graph gives six curves, three for basic displacements coming from experiment and three for FEM analysis.

The first thing to notice is that rather linear results are obtained. FEM results are perfectly linear whereas experimental ones are almost linear. One could suspect an experimental error for $F_x$ values of 20 and 30 Newtons. However, the overall behaviour is correct. Of course, all curves pass through the origin (no force, no displacement).

When comparing experimental and FEM results, it appears that FEM displacements (dotted lines) are generally under but very close to corresponding real displacements (plain lines). This seems logical because the FEM model does not take into account geometrical defaults, clearance between parts or joints stiffness. The only exception is on graph two, with $D_y$ simulated displacement which is nearly twice as great as the experimental one. This may be due to measurement errors. As shown on figures 4 and 5, dial indicators do not measure exactly TCP displacement. As for Delta-like architecture [9], given that the external force was applied under the plane defined by spherical joint centres, load in components can be lower due to the induced torque. The consequence is that machine deformation may be smaller.

Another interesting point is about coupling, *i.e.* the fact that a force along one direction may generate a displacement along another direction. Three observations can be made:

- A force along $x$ generates displacement mostly along $x$ and also along $z$ (three times smaller). This is easy to check visually on figure 10 b), where displacements are amplified 30 times.
- A force along $y$ only generates displacement along $y$. This means there is no coupling at all in this case. The phenomenon is explained clearly on figure 11, where the terminal plate has big rotations but its centre of gravity remains unchanged along $x$ and $z$. This does not appear so clearly in measured values due to parallelism errors of travelling plate lateral beams. These errors come from manufacturing and assembling errors as mentioned in section 2.

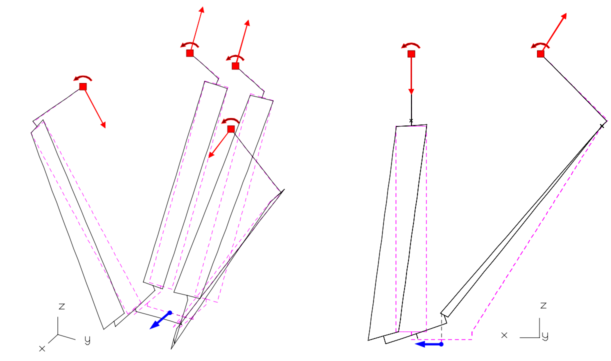

**Figure 10. Deformed structure submitted to $F_x$**

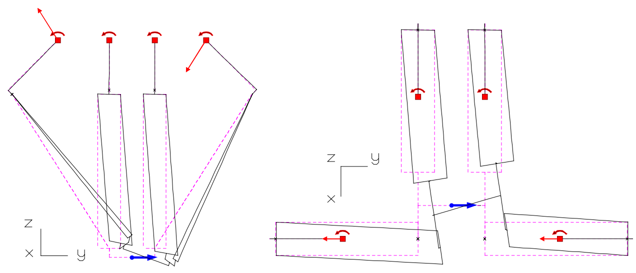

**Figure 11 Deformed structure submitted to $F_y$**

- A force along $z$ generates displacement along $x$ and also along $z$. It is rather surprising to notice that the displacement along $x$ is the biggest in this case, but the phenomenon is comparable to what can be observed on figure 10b.

Finally, curves are useful for giving the order of magnitude of stiffness along the three main directions. In the given position, it can be seen that $z$ stiffness is about twice as big as $y$ stiffness, which is about twice as big as $x$ stiffness.

This stiffness study shows that the choice of robot actuator locations on the machine frame does not provide good results. These poor results can be explained by the following analysis (see figure 12). This drawing underlines the fact that only legs 2 and 3 are stressed when a force is applied to TCP in $y$ direction. Corresponding robot element deformation only produces TCP displacement along $y$. In the other case, when the force is applied along $x$, legs 1 and 4 are stressed, this induces a force with a component along $z$ axis. To balance this force, legs 2 and 3 are also stressed. As all legs are

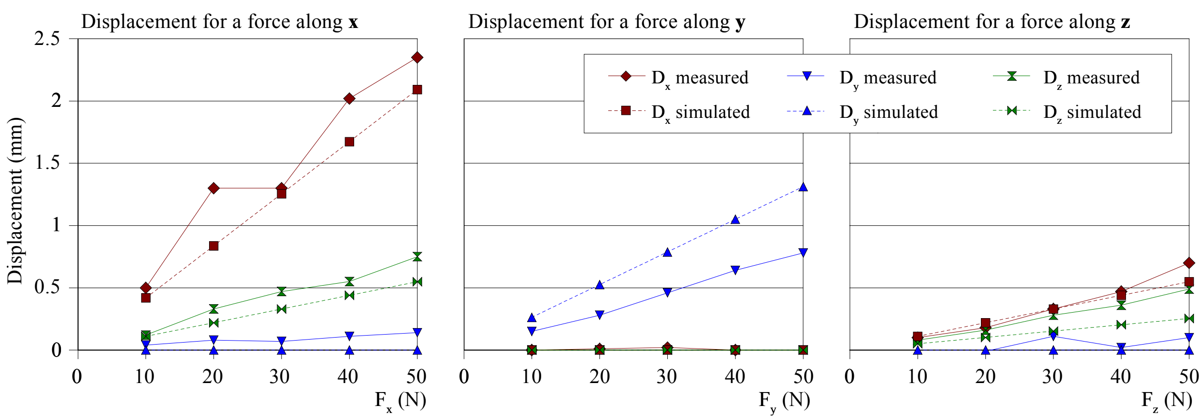


**Figure 9. Plots of measured and simulated displacements**

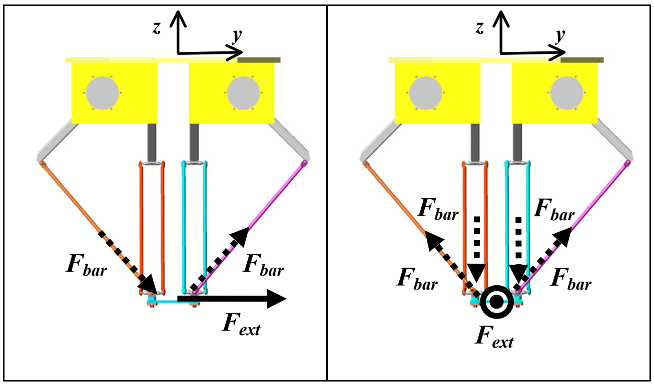


**Figure 12. Reaction to external forces on TCP**

stressed when a force is applied along $z$ axis, the resulting TCP displacement is parted between $x$ and $z$ directions ( $y$ direction is not concerned because the sum of forces along $y$ is null).

Results obtained using both methods are presented in Table 2 as two compliance matrices for our given pose. Numerical values come from the average gradient of curves on figure 9. Both matrices prove to be similar with same order magnitude.

| | Experimental | | | FEM analysis | | |
|---|---|---|---|---|---|---|
| | $D_x$ | $D_y$ | $D_z$ | $D_x$ | $D_y$ | $D_z$ |
| $F_x$ | 44 | 2 | 15 | 42 | 0 | 11 |
| $F_y$ | 0 | 16 | 0 | 0 | 26 | 0 |
| $F_z$ | 15 | 3 | 10 | 11 | 0 | 5 |

**Table 2. Compliance matrices (µm/N)**

## 6 Conclusion

This paper presented two methods to evaluate the stiffness of the H4 robot in one position close to the workspace centre (*i.e.* all actuator angles equal 45°). Results from both methods are in close agreement.

From the first analysis, it appears that the H4 robot has a different stiffness along each principal direction, with major rigidity occurring along $z$, then $y$ and then $x$ axis. Thanks to the FEM, we have a practical tool to obtain values of mechanical parameters inside the robot and also to graphically interpret its static behaviour.

It was also possible to show and to analyse various couplings between forces and displacements.

The next step will be to make stiffness maps all around the usable workspace, using classical techniques such as shown in [10] [11]. For future developments, it is also important to take into account the three angular stiffnesses that can have an influence on the robot task.

Finally, it will be possible to extract design rules from this vast amount of data and to redesign the robot. With this first glimpse on the H4 behaviour, it already seems that the actuator locations on the basement may be improved. Poor stiffness in one direction can result from two legs that work in the same direction (in this example legs 1 and 4). But it is difficult to find good actuator placement due to a geometrical condition presented in [9] that does not allow any central symmetry along $z$.

Regarding the results, the good solution for travelling plate design may be to keep the idea of two lateral beams linked to robot frame using parallelograms. Stiffness may be improved by using hyperstatic parallelograms *i.e.* made of revolute joints. As rotation is induced by beams relative motion (in that case translation), travelling plate sub-mechanism could be changed to avoid design restrictions relative to the geometrical condition mentioned above.

### Prototype dimensions

All dimensions are expressed in millimetres.

$$P_1 = \begin{bmatrix} -200 \\ -60 \\ 0 \end{bmatrix}, P_2 = \begin{bmatrix} 60 \\ -200 \\ 0 \end{bmatrix}, P_3 = \begin{bmatrix} 60 \\ 200 \\ 0 \end{bmatrix}, P_4 = \begin{bmatrix} -200 \\ 60 \\ 0 \end{bmatrix}$$

$$\boldsymbol{u_1} = -\boldsymbol{y}, \boldsymbol{u_2} = \boldsymbol{x}, \boldsymbol{u_3} = -\boldsymbol{x}, \boldsymbol{u_4} = -\boldsymbol{y}, r = 260, \ l = 480$$

$$\|B_1B_2\| = 120, \|B_3B_4\| = 120$$

$$\|A_{i1}A_{i2}\| = 60, \ \|C_1C_2\| = 120$$

### Acknowledgements

This research is funded by CNRS interdisciplinary action ROBEA MAX (CompleX Architecture Machines).

### References

1. Svinin M.M., Hosoe S., Uchiyama M., On the stiffness and Stability of Gough Stewart Platforms, In: *Proc. of 2001 IEEE International Conference on Robotics And Automation*, Seoul Korea, May 21-26, 2001
2. Pierrot F., Marquet F., Company O., Gil T., H4 parallel robot: modeling, design and preliminary experiments, In: *Proc of 2001 IEEE International Conference On Robotics and Automation*, Seoul, Korea, May 21-26, 2001
3. Pierrot F., Company O., H4: a new family of 4-DOF parallel robots, In: *AIM'99: IEEE/ASME International Conference on Advanced Intelligent Mechatronics*, Atlanta, Georgia, USA, September 19-22, 1999, pp. 508-513
4. Clavel R., A fast robot with parallel geometry, In: *Proc. of 18th Int. Symp. on Industrial Robot*, Lausanne, April 26-28, 1998, pp.91-100
5. LIRMM website, Presentation of H4 robot including video demonstration: http://www.lirmm.fr/rdc/pm/h4.html
6. Corradini C., Etude de la rigidité statique du robot à structure parallèle H4, LARAMA/IFMA Research project, June 2002, 70p.
7. Laroze S., Mécanique des structures - Théorie des poutres, Eyrolles-Masson, 1988.
8. Debard Y., RDM Ossatures - Manuel d'utilisation, February 2001, 86 p., http://iut.univ-lemans.fr/ydlogi
9. Company O., Machines outils rapides à structure parallèle. Méthodologie de conception, applications et nouveaux concepts, PHD thesis, LIRMM, UMII, December 5th, 2000, 214p.
10. Bouzgarrou C., Conception et modélisation d'une machine-outil à architecture hybride pour l'UTGV, PHD thesis, LaRAMA, IFMA, December 18th, 2001, 180p.
11. Liu X.J., Jin Z.L., Gao F., Optimum design of 3-DOF spherical parallel manipulators with respect to the conditioning and stiffness indices, In: *Mechanism and Machine Theory* 35:1257-1267, 2000